nature photonics

LETTERS

PUBLISHED ONLINE: 11 DECEMBER 2011 | DOI: 10.1038/NPHOTON.2011.296

Macroscopic non-classical states and terahertz quantum processing in room-temperature diamond

K. C. Lee[1], B. J. Sussman[2]*, M. R. Sprague[1], P. Michelberger[1], K. F. Reim[1], J. Nunn[1], N. K. Langford[1], P. J. Bustard[1,2], D. Jaksch[1,3] and I. A. Walmsley[1]*

The nature of the transition between the familiar classical, macroscopic world and the quantum, microscopic one continues to be poorly understood. Expanding the regime of observable quantum behaviour to large-scale objects is therefore an exciting open problem[1]. In macroscopic systems of interacting particles, rapid thermalization usually destroys any quantum coherence before it can be measured or used at room temperature[2]. Here, we demonstrate quantum processing in the vibrational modes of a macroscopic diamond sample under ambient conditions. Using ultrafast Raman scattering, we create an extended, highly non-classical state in the optical phonon modes of bulk diamond. Direct measurement of phonon coherence and correlations establishes the non-classical nature of the crystal dynamics. These results show that optical phonons in diamond provide a unique opportunity for the study of large-scale quantum behaviour, and highlight the potential for diamond as a micro-photonic quantum processor capable of operating at terahertz rates.

Standard quantum mechanics provides no explanation for the usual disappearance of quantum superpositions on macroscopic scales. New physics may be involved[3,4], although a broader consensus holds that thermalization with a classical environment necessarily destroys coherence[5]. Nevertheless, much recent work has investigated the quantum-classical transition in large-scale systems. For example, recent studies have suggested that quantum interference may play a functional role in living organisms where ultrafast processes, such as electron transport, benefit from quantum enhancements on timescales much shorter than the decoherence time[6]. In addition, cooled optomechanical resonators are now being developed that manifest quantum behaviour on macroscopic scales[7]. Prompted by these efforts, we generate and measure non-classical vibrational states distributed across a sample of bulk diamond using ultrafast Raman scattering. By combining the analysis of photon statistics with an ultrafast pump–probe measurement, this approach enables observation of the non-classical motion of a macroscopic solid at room temperature.

Research into generating large-scale quantum states is also motivated by their potential to revolutionize computing and communications through quantum-enhanced technologies[8,9]. In particular, quantum photonics provides a route to processing quantum information encoded in optical pulses[10]. Key requirements for a scalable photonics platform are the potential for integration and miniaturization onto chips[11], which is facilitated by operation at room temperature, in the solid state, with low optical absorption, as well as the capability to pattern the substrate. Finally, the ability to work with short optical pulses increases the clock speed of the processor and mitigates the effects of decoherence, so broadband operation is valuable. Remarkably, optical phonons in bulk diamond satisfy all these requirements, as no special preparation is required: no cooling or optical pumping; no doping or annealing. Thermal excitations at room temperature are suppressed by the high carrier frequency of the phonons. Combined with the large electronic band gap in diamond, this also permits ultra-broadband operation at all optical and near-infrared wavelengths, with minimal losses. Furthermore, waveguide structures and cavities can be etched directly in bulk diamond[12], making the implementation of complex micro-photonic circuits on-chip a feasible proposition.

Optical phonons are attractive from the perspective of quantum information processing, because they are non-propagating, persistent, coherent excitations that couple strongly to optical fields. In fact, they have all the properties necessary for a quantum memory. Quantum memories, which store propagating photons as stationary material excitations until they are needed, are an essential component for scalable photonic quantum computing[13,14]. To demonstrate the quantum nature of the phonons in diamond, we begin by implementing a quantum memory by means of off-resonant Raman scattering[15], in which an optical phonon is generated by Stokes scattering from a write pulse, with retrieval of the stored excitation stimulated by anti-Stokes scattering from a subsequent read pulse. Although the memory storage time $T \approx 7$ ps is too short for applications in long-distance quantum communications[9], the duration $\tau \approx 60$ fs of the read/write pulses is still substantially shorter, giving the memory an extremely large time–bandwidth product $B \approx T/\tau \gtrsim 100$. This is the key figure of merit for a miniaturized, chip-scale quantum memory where propagation times are negligible. One could, for instance, use several such memories to efficiently produce multiple simultaneous heralded ultrafast single photons. By appropriate timing of the read pulses, photons retrieved from the memories could be synchronized. In this context B determines the number of time bins over which randomly-emitted photons can be synchronized. The large time–bandwidth product means that diamond-based memories (with improved efficiencies, such as might be possible in an integrated architecture) could facilitate the scalable implementation of multiphoton gates in a micro-photonic quantum processor.

The Raman interaction in diamond is strong, and, because of the extremely large bandgap, has near-uniform strength at all optical wavelengths. To interpret our experiments, it is convenient to adopt a simplified picture of the diamond crystal as a three-level Λ system comprising the crystal ground state $|0\rangle$, a storage state with an excited optical phonon $|1\rangle$ and a far off-resonant intermediate state $|\text{Exciton}\rangle$ (strictly a manifold of exciton states in the conduction band; see Fig. 1a, inset). To implement a diamond quantum memory, a 60 fs write pulse (bandwidth, ~8 THz) at

[1]Clarendon Laboratory, University of Oxford, Parks Road, Oxford OX1 3PU, UK, [2]National Research Council of Canada, Ottawa, Ontario K1A 0R6, Canada, [3]Centre for Quantum Technologies, National University of Singapore, Singapore. *e-mail: ben.sussman@nrc.ca; I.Walmsley1@physics.ox.ac.uk

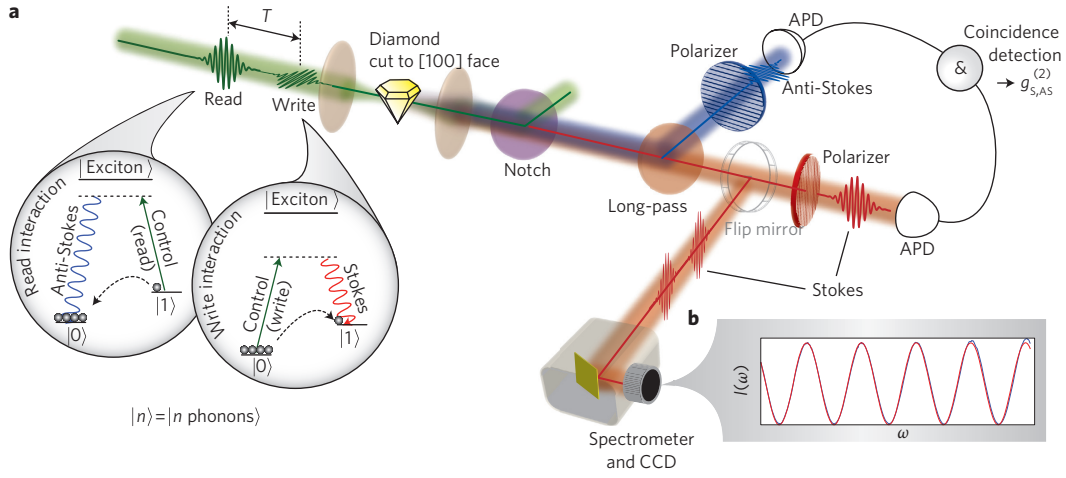

Figure 1 | Raman quantum memory and decoherence measurement in diamond. A strong write pulse simultaneously creates a Stokes photon and an optical phonon. After a delay time T, a read pulse then either scatters an additional Stokes photon (coherence measurement), or maps the phonon into an anti-Stokes pulse (quantum memory). For the coherence measurement, the read and write pulse polarizations are aligned parallel and a flip mirror directs the Stokes pulses to a photon-counting spectrometer. For the quantum memory, the read pulse is cross-polarized with respect to the write pulse, enabling separate detection of the write Stokes and read anti-Stokes photons with Geiger-mode avalanche photodiodes (APDs). The Stokes/anti-Stokes cross-correlation is calculated from the rate of coincident detection events. **a**, Simplified diamond level structure, showing Stokes and anti-Stokes scattering processes. **b**, Data showing spectral interference of the Stokes scattering probes the coherence of the phonons.

808 nm is focused into a 0.5-mm-thick diamond crystal (see Methods), followed, after a variable delay of $1 \lesssim T \lesssim 11$ ps, by a second, cross-polarized read pulse. Raman scattered light is collected, frequency and polarization filtered, and fibre-coupled to photon-counting detectors (Fig. 1). If a Stokes photon is detected from the write pulse, this heralds the creation of an optical phonon excitation: the diamond memory is now charged. After a programmable delay T, the read pulse retrieves the stored excitation, mapping it into an anti-Stokes photon.

To characterize the strength of the memory interaction, we measure the joint probability $P_{S,AS}$ of detecting both a heralding Stokes photon from the write pulse and an anti-Stokes photon from the read pulse, as well as the 'singles rates' $P_S \approx 9 \times 10^{-4}$ and $P_{AS} \approx 3 \times 10^{-6}$, which are the unconditional probabilities for detecting Stokes or anti-Stokes photons scattered from the write and read pulses, respectively. The combined collection and detection efficiency η is estimated to be ~1% for both Stokes and anti-Stokes channels. This suggests we are operating in the spontaneous scattering regime, with a scattering rate of $P_S/\eta \approx 0.1$ Stokes photons per pulse. Further support for this conclusion comes from our observation of linear scaling of P_S with write/read power, and insensitivity of the read pulse Stokes scattering to the presence of the write pulse. The probability that the write pulse generates more than one phonon is therefore small.

For a write/read delay of $T = 3$ ps (that is, time–bandwidth product $B \gtrsim 20$), we find that $P_{S,AS} \approx 9 \times 10^{-9}$. Noting the identity $P_{S,AS} = P_{AS|S} P_S$, where $P_{AS|S}$ is the conditional probability that an anti-Stokes photon is detected, given the detection of a Stokes photon, we estimate the memory retrieval efficiency—that is, the conditional probability that an anti-Stokes photon is emitted, given that the memory was successfully charged—to be $\eta_{ret} = P_{AS|S}/\eta \approx 0.1\%$. We note that the retrieval and collection efficiencies could be significantly increased in an integrated photonic architecture, to which diamond is well suited[12].

To verify the non-classical nature of the state of the diamond crystal during storage, we evaluate the normalized cross-correlation of the Stokes and anti-Stokes fields, given by $g^{(2)}_{S,AS} = P_{S,AS}/P_S P_{AS}$. Classically, the cross-correlation is upper bounded by the Cauchy–Schwarz inequality[16] $g^{(2)}_{S,AS} \leq \sqrt{g^{(2)}_{S,S} g^{(2)}_{AS,AS}}$, where the autocorrelation functions of the Stokes and anti-Stokes fields appear on the right-hand side. The Raman scattered fields are thermal with autocorrelation functions $g^{(2)}_{S,S} = g^{(2)}_{AS,AS} = 2$, so measured values of $g^{(2)}_{S,AS}$ exceeding 2 are indicative of a true quantum memory. As shown in Fig. 2, for $T = 1$ ps we observe values up to $g^{(2)}_{S,AS} \approx 5.1$, establishing that non-classical states are being stored and retrieved from the optical phonon modes in our diamond crystal.

The above results show how the excitation of an optical phonon mediates the exchange of correlations between Stokes and anti-Stokes fields that are stronger than can be explained through any classical mechanism. However, perhaps the spatial extent of the excitation quickly becomes localized, through the dephasing of neighbouring regions within the crystal. To test the global coherence of the optical phonons, we now bypass the photon-counting detectors and direct the Raman scattered light from the write and read pulses into a spectrometer. Spectral filters remove the anti-Stokes frequency, and we record the spectrum of the Stokes light; Fig. 1b shows a typical spectrum. We observe spectral fringes for which the visibility is a direct measure of the coherence of the optical phonons[17,18], which for this purpose provides a diagnostic alternative to full quantum-state tomography[19].

This can be understood as an implementation of a temporal double-slit experiment, in which a Stokes photon could have been scattered from either the write or the read pulse. Fringes are observed from the quantum-mechanical interference of the scattering amplitudes for these two indistinguishable processes. If, however, the associated phonon decays between the write and read stages, *which way* information about which pulse created the Stokes photon has leaked into the environment, and the two scattering processes become distinguishable. This in turn reduces the spectral fringe visibility. From this perspective, the observed fringes witness the quantum coherence of the phonon modes in diamond.

As shown in Fig. 3, both the Stokes spectral fringe visibility and the Stokes/anti-Stokes cross-correlation $g^{(2)}_{S,AS}$ decay as the read-write delay T is increased. The coherence lifetime T_2 of the optical phonon mode determines the lifetime of the Stokes fringes, and the population lifetime T_1 determines the lifetime of the

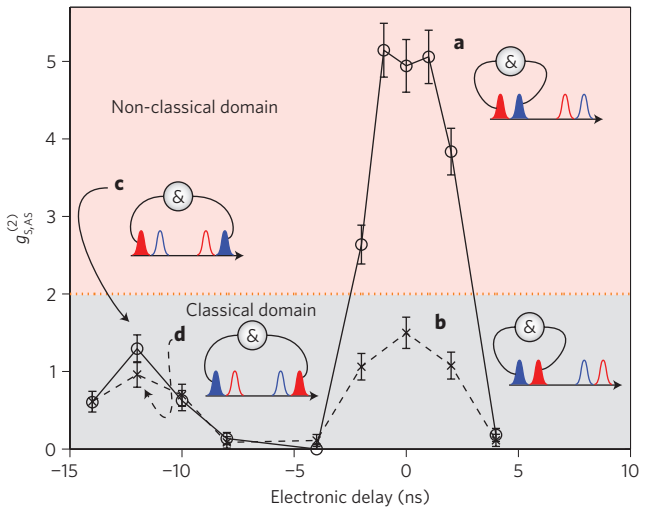

Figure 2 | Non-classical correlations in the quantum memory. a–d, The bold line shows the measured cross-correlation $g^{(2)}_{S,AS}$ for $T = 1$ ps. **a**, Violation of the Cauchy–Schwarz inequality $g^{(2)}_{S,AS} \leq 2$ confirms non-classical operation. **c**, The experiment is repeated at our laser repetition rate of 80 MHz, so that when the electronic delay is increased to 12.5 ns, accidental coincidences are measured between a write from one read–write sequence and a read from the subsequent read–write sequence, and no violations are observed. As a reference, the cross-correlation is recorded when the read and write pulses are swapped (dashed line). Only accidental coincidences are observed (**b**,**d**). The inset pulse sequences illustrate which pulses are being gated for a given electronic delay. Red pulses represent Stokes emission and blue pulses represent anti-Stokes emission. Error bars indicate standard deviations of $g^{(2)}_{S,AS}$, calculated from Poissonian photon statistics. See Methods for further details.

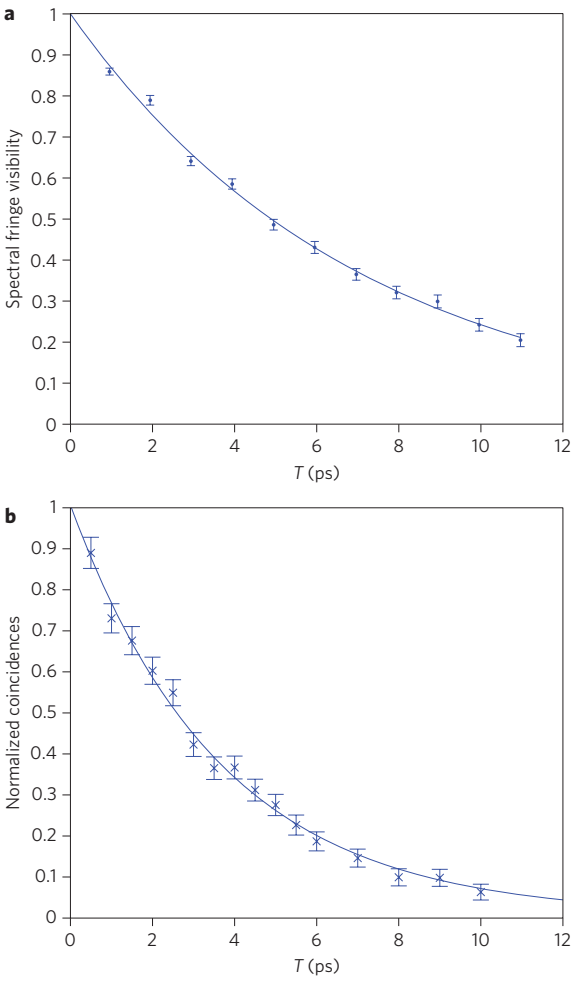

Figure 3 | Population and coherence of non-classical phonons versus read–write delay. a, The spectral fringe visibility of Stokes light monitors phonon coherence, with decay time T_2. The visibility and error bars are calculated from nonlinear regression fitting of the spectral fringes to the cosine function. **b**, Normalized $P_{S,AS}$ coincidences between write Stokes and read anti-Stokes counts measuring population decay time T_1. Error bars are calculated from Poissonian errors on the photon statistics, and the solid lines are exponential fits in both plots.

cross-correlations. The lifetimes satisfy the inequality $T_2/T_1 \leq 2$, with the ratio decreasing as pure dephasing processes decohere the phonons. We repeatably measure $T_2 \approx 6.9$ ps and $T_1 \approx 3.6$ ps, which gives a ratio $T_2/T_1 = 1.9 \approx 2$, suggesting that spectral diffusion and inhomogeneous broadening of the optical phonons can be neglected. From this we infer that the phonons remain coherent across the diamond crystal for as long as they survive. This agrees with the results of previous theoretical[20] and experimental[21] studies of Raman scattering in diamond, which concluded that the dominant decoherence mechanism for the optical phonons is the Klemens channel[22], in which optical phonons decay into pairs of acoustic phonons with equal and opposite momenta due to anharmonic coupling. Indeed, calculations based on this mechanism alone predict $T_2 \approx 11$ ps (ref. 20), which is close to our measured value. Interestingly, it is in principle possible to engineer diamond crystals with alternating layers of ^{12}C and ^{13}C, by careful manipulation of the atmosphere during chemical vapour deposition[23]. A super-lattice of these two isotopes exhibits acoustic band structure[24], and it would be possible to engineer a diamond with gaps in the acoustic phonon dispersion relation placed appropriately to forbid the Klemens channel decay. Such an approach could extend the coherence time of a diamond quantum processor, while retaining the ability to operate at room temperature. Modification of the phonon lifetime might also be achieved through controlled injection of the acoustic phonons into which the optical modes decay, as well as by changing the isotopic purity of the sample[25,26].

We have introduced optical phonons in bulk diamond as a novel quantum system, associated with the bulk vibrational modes of a macroscopic solid, the coherence of which provides access to quantum effects at room temperature. We have proposed and experimentally demonstrated a terahertz bandwidth quantum memory based on transient ultrafast Raman scattering from the optical phonons in diamond. The memory requires no optical pumping or specialized fabrication techniques, and operates at room temperature, and at all optical or near-infrared wavelengths. We confirmed the non-classical nature of the states stored in the memory by violating the Cauchy–Schwarz inequality for the Stokes/anti-Stokes cross-correlation, and we directly probed the coherence of the optical phonons using both spectral interferometry and the decay of the cross-correlation, allowing us to eliminate inhomogeneous dephasing as a decoherence mechanism. Our experiments reveal the persistence of quantum behaviour in ambient conditions, and highlight the potential of diamond as the basis for a novel solid-state architecture for ultrafast integrated micro-photonic quantum-information processing.

Methods

Source and optics. The experimental layout is described in Fig. 1. An 808 nm, full-width at half-maximum (FWHM) 60 fs Ti:sapphire oscillator was used to generate a pulse train with an 80 MHz repetition rate and an average power of 600 mW. Each pulse was split into write and read pulses, with the read pulse delayed by $1 \lesssim T \lesssim 11$ ps. The pulses were focused with a 5 cm focal length lens through a 0.5 mm diamond plate, as described below. In the chosen geometry the

Raman-scattered light was orthogonally polarized to the input, permitting selection of the output photons from either the read or write pulse by rotating the polarization of the read pulse. Notch filters removed the 808 nm read/write pulses. For the quantum memory, the Stokes and anti-Stokes beams were separated with long-pass and short-pass filters, coupled into single-mode fibres and detected with APDs that were electronically correlated in a field-programmable gate array (FPGA). To measure the coherence decay rate, a flip mirror directed the Stokes light to a 30 cm spectrometer coupled to an electron-multiplying charge-coupled device (CCD) camera.

Directional emission. Measurements of the transverse spatial profiles of the Stokes and anti-Stokes scattering, performed both with a CCD camera and in coincidence by scanning the detection fibres, revealed that they were strongly peaked in the forward direction. This directional emission—known as collective enhancement[27,28]—is a signature that the phonon mode excited in the memory is spatially coherent across the diamond sample.

The Stokes pulse was detected along the write beam direction. The read pulse propagates along the same direction and so, by symmetry, the anti-Stokes emission is in the forward direction. The process, however, is not perfectly phase-matched: the anti-Stokes retrieval efficiency $\eta_{\mathrm{ret}} = \alpha\eta_{\mathrm{ret,ideal}}$ is reduced through imperfect phasematching by a factor $\alpha = \mathrm{sinc}^2(\Delta kL/2)$, where $L = 0.5$ mm is the crystal length and Δk is the phase mismatch between the wave vector of the anti-Stokes photon and the sum of the wave vectors of the phonon and the read pulse; Δk is non-zero due to normal dispersion in the diamond. The crystal is short enough that $\alpha > 0.5$ for all frequencies in the anti-Stokes pulse propagating on-axis, but α drops rapidly for off-axis scattering. The retrieved anti-Stokes photons are therefore partially phase-matched across their entire bandwidth in the forward direction, but not phase-matched in other directions.

Diamond samples. The diamond lattice is face-centred cubic (f.c.c.), with two carbon atoms per unit cell. The space group is $Fd3m$ (O_h^7) and the crystal group $m3m$ (O_h). The optical phonon mode is triply degenerate with vibrational symmetry T_{2g} (Γ_5^+) and a first-order Raman shift of 1,332 cm^{-1} (ref. 29). The diamond sample was procured from Element 6 Ltd. and cut along the ⟨100⟩ face, resulting in Raman-scattered light polarized orthogonally to the input field. The sample was prepared by chemical vapour deposition, containing <5 parts per billion nitrogen impurity and a dislocation density of $\sim 10^3$–10^4 cm^{-2}. Photoluminescence images showed sparsely populated blue lines signifying the presence of dislocations, which are known to emit over a broad bandwidth (the 'A-band') centred at 435 nm (ref. 30). Interestingly, these localized imperfections do not appear to affect the functioning of the memory.

Received 15 June 2011; accepted 26 October 2011; published online 11 December 2011

References

1. Aspelmeyer, M., Gröblacher, S., Hammerer, K. & Kiesel, N. Quantum optomechanics—throwing a glance. *J. Opt. Soc. Am. B* **27,** A189–A197 (2010).
2. Zurek, W. Pointer basis of quantum apparatus: into what mixture does the wave packet collapse? *Phys. Rev. D* **24,** 1516–1525 (1981).
3. Milburn, G. Intrinsic decoherence in quantum mechanics. *Phys. Rev. A* **44,** 5401–5406 (1991).
4. Ellis, J., Mohanty, S. & Nanopoulos, D. Quantum gravity and the collapse of the wavefunction. *Phys. Lett. B* **221,** 113–119 (1989).
5. Strunz, W., Haake, F. & Braun, D. Universality of decoherence for macroscopic quantum superpositions. *Phys. Rev. A* **67,** 022101 (2003).
6. Gauger, E., Rieper, E., Morton, J., Benjamin, S. & Vedral, V. Sustained quantum coherence and entanglement in the avian compass. *Phys. Rev. Lett.* **106,** 40503 (2011).
7. Cho, A. Faintest thrum heralds quantum machines. *Science* **327,** 516–518 (2010).
8. Knill, E., Laflamme, R. & Milburn, G. J. A scheme for efficient quantum computation with linear optics. *Nature* **409,** 46–52 (2001).
9. Sangouard, N., Simon, C., de Riedmatten, H. & Gisin, N. Quantum repeaters based on atomic ensembles and linear optics. *Rev. Mod. Phys.* **83,** 33–80 (2011).
10. Walmsley, I. Looking to the future of quantum optics. *Science* **319,** 1211–1213 (2008).
11. Smith, B. J., Kundys, D., Thomas-Peter, N., Smith, P. G. R. & Walmsley, I. A. Phase-controlled integrated photonic quantum circuits. *Opt. Express.* **17,** 13516–13525 (2009).
12. Faraon, A., Barclay, P. E., Santori, C., Fu, K.-M. C. & Beausoleil, R. G. Resonant enhancement of the zero-phonon emission from a colour centre in a diamond cavity. *Nature Photon.* **5,** 301–305 (2011).
13. Lvovsky, A., Sanders, B. & Tittel, W. Optical quantum memory. *Nature Photon.* **3,** 706–714 (2009).
14. Hammerer, K., Sørensen, A. & Polzik, E. Quantum interface between light and atomic ensembles. *Rev. Mod. Phys.* **82,** 1041–1093 (2010).
15. Jiang, W., Han, C., Xue, P., Duan, L. & Guo, G. Nonclassical photon pairs generated from a room-temperature atomic ensemble. *Phys. Rev. A* **69,** 043819 (2004).
16. Loudon, R. *The Quantum Theory of Light* (Oxford Univ. Press, 2004).
17. Waldermann, F. *et al.* Measuring phonon dephasing with ultrafast pulses using Raman spectral interference. *Phys. Rev. B* **78,** 155201 (2008).
18. Lee, K. C. *et al.* Comparing phonon dephasing lifetimes in diamond using transient coherent ultrafast phonon spectroscopy. *Diam. Rel. Mater.* **19,** 1289–1295 (2010).
19. Lobino, M., Kupchak, C., Figueroa, E. & Lvovsky, A. Memory for light as a quantum process. *Phys. Rev. Lett.* **102,** 203601 (2009).
20. Debernardi, A., Baroni, S. & Molinari, E. Anharmonic phonon lifetimes in semiconductors from density-functional perturbation theory. *Phys. Rev. Lett.* **75,** 1819–1822 (1995).
21. Liu, M., Bursill, L., Prawer, S. & Beserman, R. Temperature dependence of the first-order Raman phonon line of diamond. *Phys. Rev. B* **61,** 3391–3395 (2000).
22. Klemens, P. Anharmonic decay of optical phonons. *Phys. Rev.* **148,** 845–848 (1966).
23. Balasubramanian, G. *et al.* Ultralong spin coherence time in isotopically engineered diamond. *Nature Mater.* **8,** 383–387 (2009).
24. Catellani, A. & Sorba, L. Acoustic-wave transmission in semiconductor superlattices. *Phys. Rev. B* **38,** 7717–7722 (1988).
25. Hass, K. C., Tamor, M. A., Anthony, T. R. & Banholzer, W. F. Lattice dynamics and raman spectra of isotopically mixed diamond. *Phys. Rev. B* **45,** 7171–7182 (1992).
26. Chrenko, R. ^{13}C-doped diamond: Raman spectra. *J. Appl. Phys.* **63,** 5873–5875 (1988).
27. Duan, L., Cirac, J. & Zoller, P. Three-dimensional theory for interaction between atomic ensembles and free-space light. *Phys. Rev. A* **66,** 023818 (2002).
28. Sørensen, M. & Sørensen, A. Three-dimensional theory of stimulated Raman scattering. *Phys. Rev. A* **80,** 033804 (2009).
29. Hayes, W. & Loudon, R. Scattering of Light by Crystals (Dover Publications, 2004).
30. Hornstra, J. Dislocations in the diamond lattice. *J. Phys. Chem. Solids* **5,** 129–141 (1958).

Acknowledgements

This work was supported by the QIPIRC (Quantum Information Processing Interdisciplinary Research Collaboration) and EPSRC (Engineering and Physical Sciences Research Council) (grant no. GR/S82176/01), EU ITN (European Union International Training Network) EMALI (Engineering, Manipulation and Characterization of Quantum States of Matter and Light), EU IP (Integrated Project) Q-ESSENCE (Quantum Interfaces, Sensors, and Communication based on Entanglement), EU ITN FASTQUAST (Ultrafast Control of Quantum Systems by Strong Laser Fields), Toshiba Research Europe, Clarendon Fund, NSERC (Natural Sciences and Engineering Research Council of Canada), and a Royal Society/Wolfson Research Merit Award. The authors are grateful to S. Prawer for useful discussions.

Author contributions

K.C.L. built the experiment with assistance from B.J.S. and M.R.S. and collected the data. K.C.L., B.J.S. and J.N. contributed to the theoretical analysis. K.F.R., P.M., N.K.L., P.J.B. and D.J. provided useful insights, and I.A.W. and B.J.S. conceived the experiment. The manuscript was written by K.C.L. with input from B.J.S., J.N., N.K.L., M.R.S. and I.A.W.

Additional information

The authors declare no competing financial interests. Reprints and permission information is available online at http://www.nature.com/reprints. Correspondence and requests for materials should be addressed to B.J.S. and I.A.W.